Flare SOL2012-07-06: on the origin of the circular polarization reversal between 17 GHz and 34 GHz

A. Altyntsev[1] · **N. Meshalkina**[1] ·
I. Myshyakov[1] · **V. Pal'shin**[2] ·
G. Fleishman[3,2] ·

Abstract The new generations of multiwavelength radioheliographs with high spatial resolution will employ microwave imaging spectropolarimetry to recover flare topology and plasma parameters in the flare sources and along the wave propagation paths. The recorded polarization depends on the emission mechanism and emission regime (optically thick or thin), the emitting particle properties, and propagation effects. Here, we report an unusual flare, SOL2012-07-06T01:37, whose optically thin gyrosynchrotron emission of the main source displays an apparently ordinary mode sense of polarization in contrast to the classical theory that favors the extraordinary mode. This flare produced copious nonthermal emission in hard X-rays and in high-frequency microwaves up to 80 GHz. It is found that the main flare source corresponds to an interaction site of two loops with greatly different sizes. The flare occurred in the central part of the solar disk, which allows reconstructing the magnetic field in the flare region using vector magnetogram data. We have investigated the three possible known reasons of the circular polarization sense reversal – mode coupling, positron contribution, and the effect of beamed angular distribution. We excluded polarization reversal due to contribution of positrons because there was no relevant response in the X-ray emission. We find that a beam-like electron distribution can produce the observed polarization behavior, but the source thermal density must be much higher than the estimate from to the X-ray data. We conclude that the apparent ordinary wave emission in the optically thin mode is due to radio wave propagation across the quasi-transverse (QT) layer. The abnormally high transition frequency (above 35 GHz) can be achieved reasonably low in the corona where the magnetic field value is high and transverse to the line of

[1] Institute of Solar-Terrestrial Physics SB RAS, Lermontov st. 126A, Irkutsk 664033, Russian Federation email: altyntsev@iszf.irk.ru email: nata@iszf.irk.ru email: ivan_m@iszf.irk.ru
[2] Ioffe Physical Technical Institute, St. Petersburg, 194021, Russian Federation email: e.mail-a email: val@mail.ioffe.ru
[3] Center For Solar-Terrestrial Research, New Jersey Institute of Technology, Newark, NJ 07102 email: e.mail-a email: gfleishm@njit.edu

sight. This places the microwave source below this QT layer, *i.e.* very low in the corona.

Keywords: Radio Emission, Solar; Polarization; X-Ray Bursts, Flares

1. Introduction

The generation of high-energy charged particles in solar flares remains an outstanding, high-priority problem of solar physics. Many competing acceleration mechanisms have been proposed and compared with various data sets, but no ultimate choice has been made in favor of one or only a few mechanisms. The flare microwave emission of mildly relativistic electrons can help to distinguish these acceleration mechanisms as it provides us with important information on plasma and nonthermal particles in the flare region, and coronal plasma properties along the wave path.

The spatially resolved data of the Stokes I and V components are available from a number of solar radio instruments at different microwave frequencies, such as the *Nobeyama Radioheliograph* (NoRH, Nakajima *et al.*, 1994), the *Siberian Solar Radio Telescope* (SSRT, Grechnev *et al.*, 2003), and *Owens Valley Solar Arrays* (OVSA, Gary and Hurford, 1994). A new generation of microwave multi'wavelength radioheliographs is now under various stages of development: the expanded OVSA (Gary *et al.*, 2012), the *Frequency Agile Solar Radiotelescope* (FASR, Bastian, 2004), the *Mingantu Ultrawide Spectral Radioheliograph* (MUSER, Yan *et al.*, 2013) and the *Siberian Radio Heliograph* (SRH, Lesovoi *et al.*, 2014; 2017).

Gyrosynchrotron sources at high frequencies are often located close to the flare loop footpoints where the magnetic field exceeds several hundred Gauss, before lower frequencies are emitted from greater heights. Flares initiated by an interaction of two loops of rather different size have been reported (Hanaoka, 1997; Nishio *et al.*, 1997; Altyntsev *et al.*, 2016; Fleishman *et al.*, 2016). The NoRH polarization images at 17 GHz showed footpoints of a small loop and the SSRT observed a large loop at 5.7 GHz. The main microwave and X-ray sources were located in or close to the site of the loop–loop interaction.

The measured polarization of the microwave sources depends on intrinsic polarization at the emission source and its modification through propagation effects. The intrinsic polarization is determined by the emission mechanism and emission regime (*e.g.*, optically thin or thick regimes), the emission 'driver' properties, *e.g.*, the type of radiating particles (electrons or positrons) or their angular distribution, and the source properties, *e.g.*, the strength and orientation of the magnetic field. It is known that the continuum microwave emission of solar flares is primarily generated by the nonthermal electrons through the gyrosynchrotron emission mechanism (Ramaty, 1969). The gyrosynchrotron emissivity increases with the magnitude of the magnetic field. A compact microwave high–frequency source is therefore expected to appear at the loop footpoint, where the nonthermal particles precipitate and the magnetic field is enhanced. Emission from these sources is circularly polarized, and the sign of the polarization is determined by the direction of the magnetic field at the source.

In the case of an isotropic distribution of emitting electrons the gyrosynchrotron mechanism favors the extraordinary mode in the optically thin regime at high frequencies. Thus, the source located at the footpoint of a loop rooted in the north (positive) polarity magnetic field should be seen as the right–hand circular polarization (RCP) source (Dulk and Marsh, 1982; Bastian, 1998). In some cases, however, the microwave source can favor the ordinary waves. First of all, the optically thick polarization at frequencies below the spectrum peak is polarized in the sense of the ordinary mode. In the optically thin regime, the sense of polarization can correspond to the ordinary wave mode for a certain range of viewing angles for beamlike distributions of emitting nonthermal electrons (Fleishman and Melnikov, 2003). Such an event with a polarization reversal at high frequencies, which corresponds to ordinary–mode emission, was found by Altyntsev *et al.* (2008) and recently by Morgachev *et al.* (2014) and the reversal was explained by the strong anisotropy in the electron pitch–angle distribution. Then, Fleishman *et al.* (2013) proposed that waves with the sense of the ordinary wave can be generated at high frequencies by relativistic positrons if their differential energy spectrum at high energies exceeds that of the electrons.

The importance of propagation effects was discovered a long time ago (Cohen, 1960; Zheleznyakov and Zlotnik, 1963; Alissandrakis *et al.*, 1993). A circularly polarized wave reverts its helicity when it propagates through a quasi–transverse region, where the directions of ray propagation and of the magnetic field are orthogonal. If the mode coupling is weak the polarization continuously adjusts itself to the local polarization state for the mode in question. If the mode coupling is strong, there is no change in the state of polarization of radiation through propagation effects. Cohen (1960) defined the transition frequency f_t such that for $f \gg f_t$ ($f \ll f_t$) the coupling is strong (weak). The polarization reversals are used to probe the corona (see, *e.g.* Lee *et al.*, 1998; Ryabov *et al.*, 2005).

The NoRH images at 17 GHz of the Stokes I and V components are currently the most suitable images for studying polarization effects because this frequency typically corresponds to the optically thin regime and is expected to be not strongly affected by the mode coupling. The NoRH images have high spatial resolution and have been intensively studied by solar astronomers for more than twenty years. Until recently, only very few studies paid particular attention to the radio polarization observed by the NoRH, however. Huang and Nakajima (2009) published a statistical analysis of the flaring loops. As mentioned above it is theoretically predicted that the gyrosynchrotron emission is dominated by the extraordinary mode. The footpoints of loops should be located on the south (negative) and north (positive) magnetic field and the emission of the conjugate points must have the opposite sense of circular polarization. Most of the analyzed events had the same polarization sense at both footpoints, however. Huang and Nakajima (2009) did not study this effect in detail, but have emphasized that the polarization of the microwave burst was strongly affected by propagation effects through the overlying magnetic field, such as linear mode conversion.

Thus the study of the polarization and its reversals is a potentially powerful, but yet largely unexplored, diagnostic tool. Of particular interest is the study of events recorded by the *Nobeyama Radio Polarimeters* (NoRP, Torii *et al.*, 1979) with opposite senses of circular polarization at 17 and 35 GHz. Fleishman et al.

(2013) have recently searched the entire Nobeyama database until 2013 and have found that such a reversal was observed for about 1% of all microwave bursts recorded by the Nobeyama instruments.

This article analyzes the M2.9 impulsive flare on 2012 July 6 at 01:38 UT, in which the microwave burst was oppositely circularly polarized at 17 and 35 GHz. The flare sources in X–rays and microwaves were separated by a distance sufficient to resolve them in the RHESSI and Nobeyama images. The event occurred reasonably close to the disk center to allow reconstructing the magnetic field in the flare region. In the flash (impulsive) phase of the flare a significant burst was observed in microwaves up to 80 GHz, and in X–rays in the range of up to 300–800 keV.

2. Instruments and observations

Microwave total fluxes were recorded with the *Nobeyama Radio Polarimeters* in intensity $I = R + L$ and circular polarization $V = R - L$ at six frequencies (1, 2, 3.75, 9.4, 17, and 35 GHz) and in the intensity only at 80 GHz with a time resolution of 0.1 sec, and in 1 s intensity data from the *Radio Solar Telescope Network* (RSTN, Guidice *et al.*, 1981) at seven frequencies (0.4, 0.6, 1.4, 2.7, 5.0, 8.8, and 15.4 GHz). To measure the spectrum, we also used data from the *Solar Radio Spectropolarimeters* (SRS) (I and V fluxes at 16 frequencies: 2.3, 2.6, 2.8, 3.2, 3.6, 4.2, 4.8, 5.6, 6.6, 7.8, 8.7, 10.1, 13.2, 15.7, 19.9, and 22.9 GHz; the temporal resolution is 1.6 s) that have been created by the SSRT team.

The microwave imaging was performed with the SSRT (Grechnev *et al.*, 2003) at 5.7 GHz (intensity and polarization) and the NoRH (Nakajima *et al.*, 1994) at 17 GHz (intensity and polarization) and 34 GHz (intensity only). The NoRH spatial resolution was 13 arcsec at 17 GHz and 8 arcsec at 34 GHz. We used the imaging with 1 s cadence. The 17 GHz fluxes in intensity and polarization obtained from the NoRH images are close to the NoRP data. The 35 GHz intensity flux measured by the NoRP is 1.9 times higher than the flux calculated from the NoRH images at 34 GHz, however. We have found that the NoRH disk–fitting was sufficiently reliable before the burst maximum. At the maximum, the partial images showed the reliable temperature of the quiet Sun as well. We therefore reduced the NoRP fluxes at 35 GHz in intensity and polarization using this factor. This correction does not affect the values of the polarization degree.

The SSRT is a cross–shaped interferometer and the data recorded by the east–west (EW) and north–south (NS) arrays provide two–dimensional images of the solar disk every two to three minutes and one–dimensional images (scans) every 0.3 s in the standard mode of the observations. The receiver system of SSRT contains a spectrum analyzer with 250 frequency channels, which corresponds to the knife–edge–shaped fan beams for the NS and EW arrays. The response at each frequency corresponds to the emission from a narrow strip on the solar disk whose position and width depend on the observation time, array type, and frequency. The signals from all the channels are recorded simultaneously and generate a one–dimensional distribution of solar radio brightness. In this study we use the one–dimenshional images provided by the EW linear antenna array.

The width of the EW beam was 26 arcsec and the receiving strip was made at an angle of 28 degrees counterclockwise relative to the central solar meridian.

We used the HXR data obtained with the RHESSI (Lin *et al.*, 2002). For imaging we used the forward–fit (FWD) method and for spectrum calculations – we used the OSPEX package. The FWD approach is rather effective for sources with a relatively simple structure such as the one we study here. HXR and gamma–ray data for this event were also obtained with the *WIND*/KONUS spectrometer (Aptekar *et al.*, 1995; Palshin *et al.*, 2014).

To study structure of the flare region we use the EUV images obtained with the *Atmospheric Imaging Assembly* (AIA, Lemen *et al.*, 2012) onboard the *Solar Dynamics Observatory* (SDO). For the boundary conditions, the 12–minute full–Sun vector magnetograms obtained by the SDO/HMI instrument (Scherrer *et al.*, 2012) were used.

Light curves recorded in the flash stage with the NoRH and the RHESSI are presented in Figure 1. The duration and behavior of the HXR signals were strongly different at energies above and below 25 keV. The shortest signals of 10–15 s duration were observed at high energies. At low energies the flux started to grow smoothly before and reached the maximum a minute after the impulsive peak. Note that the behavior of the hard X–rays with energies lower than 12 keV is similar to that of the plasma temperature provided by the GOES data. The temperature reached 20 MK at 01:39:37 UT.

Microwave emission was observed in a wide range of frequencies up to 80 GHz, which is the highest working frequency of the Nobeyama spectropolarimeters. The light curves at high frequencies were similar to the hardest X–ray ones. The maximum radio flux was observed at 17 GHz and reached 730 SFU at 01:38:50 UT. The duration of the high–frequency burst at 35 – 80 GHz was the same as that of the hard X–ray burst. At frequencies below 17 GHz, the microwave light curves became smoother with a relatively slower rise and decay. The polarization profiles at frequencies below 35 GHz were left–handed during the impulsive phase. The polarization degree did not exceed a few percent. At 35 GHz, the polarization profile was right–handed and showed a short pulse similar to the intensity pulse, and the degree of polarization was $V/I = 0.1 - 0.35$. The 80 GHz data do not have polarization information.

Spectral properties. The ratio of the RHESSI signals at 100–300 keV and 50–100 keV shows a soft–hard–soft behavior. Using the OSPEX procedure we found that the hard X–ray photons with energies up to 600 keV can be described as $2.22 \times (E/50)^{-3.0}$ ph/(s·cm²keV) at flux maximum. The *Wind*/KONUS spectrum $2.15 \times (E/50_{keV})^{-3.2}$ ph/(s·cm²keV) is consistent with the spectrum of RHESSI. We searched for an annihilation line and found that the light curves recorded by both instruments do not show any noticeable enhancement above the background at 511 keV during the flash phase.

The microwave spectra are shown in Figure 2. Note the high consistency of the spectral data from the different spectrographs. The spectrum shapes are typical for gyrosynchrotron emission. The spectral peak frequency was varying around 17 GHz and was higher at time peaks 3 and 4. The emission at 35 and 80 GHz clearly corresponds to the optically thin regime.
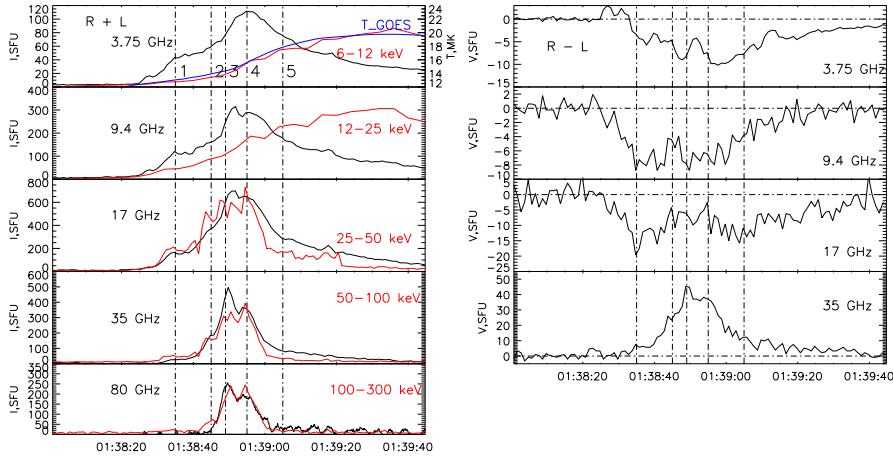
Figure 1. Lightcurves of X–ray (RHESSI, *red*) and microwave fluxes (NoRP, *black*) in intensity ($R+L$, *left*) and in polarization ($R-L$, *right*). Plasma temperature profile calculated from the GOES data are shown in the left top panel. The RHESSI data are presented in arbitrary units.
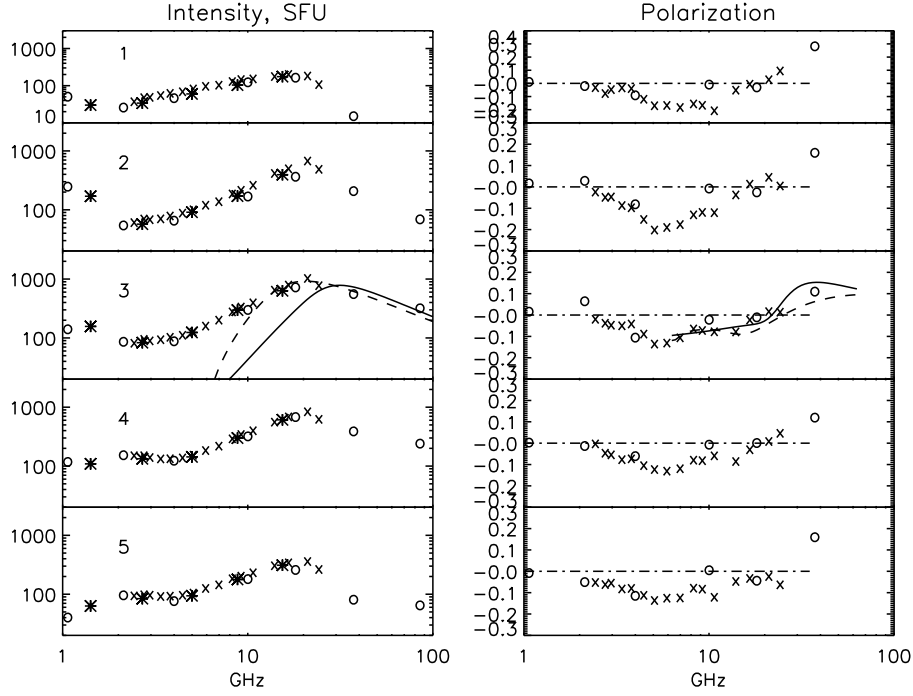

Figure 2. Microwave spectra in intensity (left) and polarization degree (right) for the time frames marked in Figure 1. The data were recorded by the RSTN (asterisks), NoRP (circles) and the SRS spectropolarimeters (crosses). In panel 3 the results of fitting the high–frequency part are shown by the solid and dashed curves for the isotropic and anisotropic case, respectively.

The spectra of the circular polarization degree for the same time frames are shown in the right panels. Mainly left–handed emission reaches the level of 0.1–0.2 at 5–7 GHz. At the frequencies above 17 GHz the polarization sense reversal was observed at both spectropolarimeters: NoRP and SRS. At 35 GHz the polarization degree varied from 0.25 down to 0.1. If the angular distribution of the emitting electrons is isotropic, a behavior of the circular polarization sense like this is expected for a source located above the N–polarity region.

Flare configuration. The flare occurred in the very flare–productive Active Region 11515 (S17W50). More than twenty flares were observed on the day before the event under study (including M–class flares). Microwave and X–ray sources aligned with a cotemporal SDO/HMI magnetogram are shown at the peak time of the burst in Figure 3. The bulk of the emission was observed from source 1, where the X–ray and 34 GHz sources and the brightness centers of emission at 17 GHz were located. Microwave source 1 was left–handedly polarized at 17 GHz. There were two more flare sources, located to the northwest (source 2) at a distance of 15 arcsec and 90 arcsec eastward (source 3). Source 2 is detected in polarization because of the opposite sense, *i.e.* it was right handed.

LCP source 3 occurred during the flare above an S–polarity region. Figure 3 shows the contours of the first image at 5.7 GHz, which was not overexposed and was recorded at 01:41 UT. There are two bright regions corresponding to source 3 and the region that combines sources 1 and 2 because the spatial resolution was too low to resolve them. The one–dimensional scans show that a significant emission at 5.7 GHz was generated in the loops connecting source 3 with the region spanning sources 1 + 2.

The extended region with sources 1 and 2 is shown in Figure 4. The background 335 Å image corresponds to a time frame in which the EUV images were not saturated and the post–flare loop was clearly seen. The EUV loop connected a narrow S–polarity intrusion to a vast area of N polarity. The brightness center of 34 GHz emission was located in the S–polarity strip. The 17 GHz RCP source 2 was located in this N–polarity region with a magnetic field $B > 500$ G, the brightness center of the LCP source was in close proximity to the strip of S polarity. The distance between the sources was about 15 arcsec. The apparent sizes of microwave sources 1 are close to the NoRH beam FWHM: 13 arcsec at 17 GHz and 8 arcsec at 34 GHz. Thus the real sizes of the sources did not exceed a few arcseconds.

A microwave source at 17 GHz in the place of source 1 appeared two days before the flare and changed its polarization from RCP to LCP on 5 July (Figure 5). The source brightness temperature was increasing from 80 000 K up to a few 100 000 K at 01:37:31 UT on July 6.

To reveal links between the sources during the flare we made a so–called mean square (RMS) map using the 17 GHz images in polarization (see, *e.g.* Grechnev, 2003). The sources are marked by the white–black dotted contours that corresponded to the half–width of the RMS brightness temperature variances (Figure 3). The time profiles for each microwave source are shown in Figure 6. There was an impulsive component in the emission from source 2, and a gradual component in the emission from source 3. The polarization degrees of the emission from the two weak sources reached high values of 50% and more.
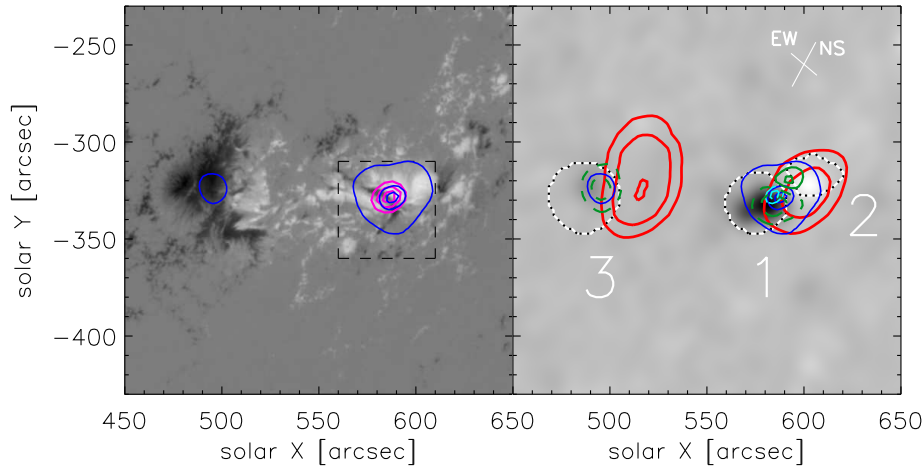
Figure 3. Flare structure. The grayscale background is a magnetogram taken at 01:39:00 UT (left panel) and an RMS polarization map at 17 GHz (right). Blue contours mark the 17 GHz sources in intensity (levels $0.016, 0.6, 0.9) \times 120$ MK at 01:38:48 UT. In the left panel the pink contours present the HXR brightness levels at 25–50 keV (0.3, 0.6, 0.9, RHESSI) relative to maximum (averaged over 01:38:49 – 01:38:54 UT). Right panel: the black–white contours bound the masks for flare sources, marked by numbers; red contours $(0.5, 0.7, 0.99) \times 142$ MK show the intensity of microwave sources at 5.7 GHz (01:41 UT), and cyan contours $(0.6, 0.9) \times 9$ MK – 34 GHz. Green contours present the 17 GHz emission in polarization at 01:38:48 UT: the dashed – LCP, levels $(0.2, 0.6) \times 3.4$ MK) and solid lines show RCP, levels $(0.3, 0.9) \times 0.6$ MK). In the top right corner the cross presents directions and beam width of the one–dimensional SSRT scans. The extended frame (dashed black square in the left panel) is shown in Figure 4.

The polarization degree of source 1 was about 5% at 17 GHz. The brightening of source 2 during the flare and the opposite sense of circular polarization relative to main flare source 1 confirm that sources 1 and 2 correspond to the footpoints of a flare loop.

The solid profile in the 4th panel in Figure 6 shows the 34 GHz flux emitted from source 1 and the dashed curve presents the flux from outside this source. The outside flux was rather small and the emission was almost entirely produced by source 1. We therefore conclude that the total power flux recorded with the NoRP at 35 GHz only contains contribution only from source 1. Here we suggest that the emission properties at 34 GHz (NoRH) and 35 GHz (NoRP) are the same.

Although the accuracy of the NoRH image coalignment with the magnetogram (about 10 arcsec) is comparable with the S–intrusion width we believe that the data on the flare configuration allow us to associate source 1 with the S–polarity region. The value of the photospheric magnetic field at the 34 GHz source site was about 1 kG. Data on thermal X–rays were provided by the GOES and low–energy RHESSI channels. During the impulsive phase the emission measure was estimated from the GOES data as 5.3×10^{48} cm^{-3}. In the RHESSI data this value is twice as high. For an X–ray source size of 10 arcsec we estimate the density of the source plasma to be $(6 - 10) \times 10^{10}$ cm^{-3}.
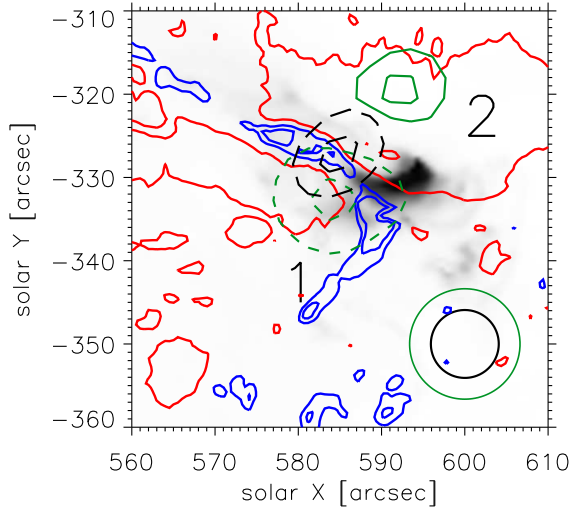
Figure 4. Flare sources 1 and 2. Background: AIA/SDO 335 Å negative image at 01:40:38 UT. The LOS magnetogram of HMI/SDO at 01:39:00 UT is shown with blue contours at –500, –150 G and red contours at 500, 1500 G. The black dashed contours show the 34 GHz source at $(0.5, 0.9) \times 46$ MK (01:38:48 UT). The brightness temperatures at 17 GHz are shown for LCP $(0.5, 0.9) \times 3.4$ MK (green dashed contours) and RCP, $(0.5, 0.9) \times 0.6$ MK (green solid contours). The FWHM of the NoRH beams at (green) and 34 GHz (yellow) are shown in the right bottom corner.

Figure 5. Evolution of sources 1 and 2 at 17 GHz. The grayscale background is the intensity. Contours correspond to RCP (solid) and LCP (dashed) emission. Levels 0.1, 0.5, and 0.9 are relative to the corresponding brightness maximum. Coordinates are given in arcseconds from the solar center.

3. Discussion

The flare under study demonstrates significant nonthermal particle signatures with delayed thermal emission. The flare is initiated by interaction between a small loop and a large loop. The interaction site, seen as the main source in hard X–rays and in microwaves, is located near the common footpoint of the loops. Recently such flares have been discussed by Altyntsev *et al.* (2016) and Fleishman *et al.* (2016).
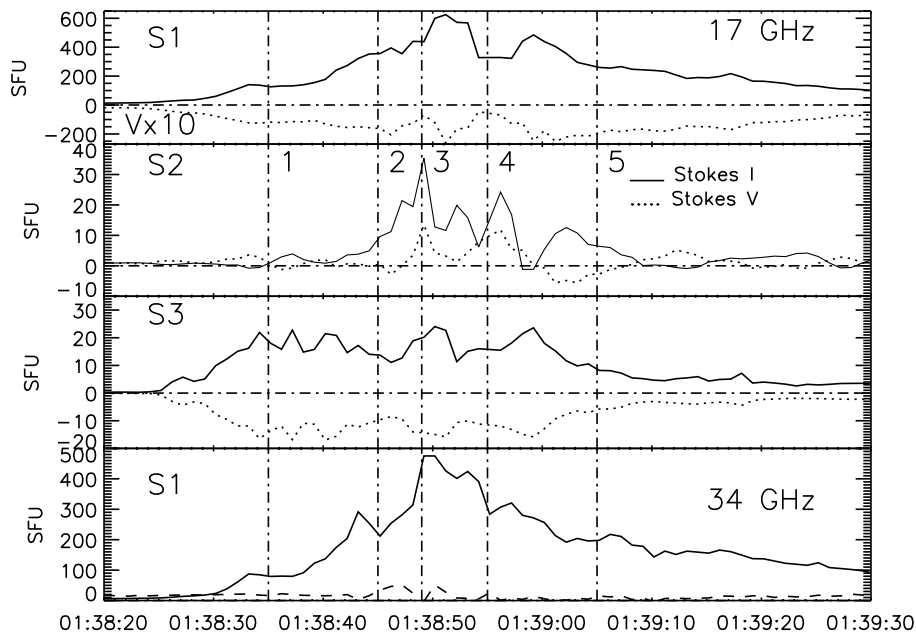
Figure 6. Microwave fluxes from the flare sources marked in Figure 3. In the bottom panel the solid curve corresponds to emission from source 1 bounded by the black–white contour in Figure 3, and the dashed curve shows the profile of flux emitted outside the source.

In our event the spatial observations showed that almost all of the emission at the NoRH frequencies (17 and 34 GHz) comes from source 1. It is shown that their microwave emission changes the polarization sense between 17 and 35 GHz. We argued that this source is located above a narrow S–polarity channel within a large N–polarity region. The polarization sense reversal above 17 GHz therefore corresponds to the transition from the extraordinary to the ordinary wave. Such reversal is opposite to what we expect at crossing through the spectral peak frequency while the spectrum transits from the optically thick to the thin regime.

There are two ways to generate the ordinary–mode polarization at high frequencies in the framework of the gyrosynchrotron emission mechanism. The first way has recently been proposed by Fleishman *et al.* (2013): emission by relativistic positrons. Indeed, if the flare emission at high frequencies is primarily produced by high–energy positrons rather than electrons the polarization will correspond to the ordinary wave mode. The corresponding light curves recorded with the RHESSI and *Wind*/KONUS spectrometers show that there was no annihilation line that would be indicative of the flare positrons during the event under study. The possibility of producing microwave emission by positrons was first pointed out by Lingenfelter and Ramaty (1967). Trottet *et al.* (2008) found a

close correlation in time and space of radio emission at 210 GHz with the production of pions during the 2003 October 28 flare. However, an order–of–magnitude estimate of possible positron numbers consistent with an X–ray non–detection of the positron annihilation line rather suggests that the numbers of positrons are far too small to account for the observed radio emission. Thus we have no evidence in support of the positron hypothesis in this flare.

The other possibility to generate the ordinary–mode emission from the optically thin source is through pitch–angle anisotropy of the emitting electrons (Fleishman and Melnikov, 2003). To test this possibility, we simulated the high–frequency part of the spectra using a uniform source model with the gyrosynchrotron (GS) fast codes developed by Fleishman and Kuznetsov (2010). We found that the polarization reversal at frequencies above 17 GHz can indeed be achieved for some angular distributions of emitting electrons. Specifically, to obtain the polarization reversal as observed we used the distributions with a Gaussian pitch–angle anisotropy given by the expression: $g(\mu) \sim \exp[-(\mu - \mu_0)^2)/\Delta\mu^2]$, where $\mu_0 = \cos\alpha_0$ is the beam direction, and $\Delta\mu$ is the beam angular width. This expression represents the beam along the field line for $\mu_0 = \pm 1$, the transverse beam for $\mu_0 = 0$, and an oblique beam (or a hollow beam) otherwise.

One of the best 'by eye' fits is shown by the dashed curve in Figure 2 (panel 3). In this example the polarization dependence on frequency is similar to the observed dependence at frequencies above 7 GHz. The parameters of the best–fit angular distribution are a source size of $10 \times 10 \times 10$ arcsec, a plasma density and temperature of 20 MK and 3×10^{11} cm^{-3}, a power–law index of $\delta_{MW} = 3.5$, a density of the nonthermal electrons of 9×10^7 cm^{-3}, a magnetic field of 480 G, a viewing angle of 83°, $\Delta\mu = 0.4$, and a beam direction $\alpha_o = 60^o$. The electron index δ_{MW} is consistent with the X–ray flux index $\gamma_X = 3.0-3.2$. Simulations show a strong dependence of the polarization spectrum on the anisotropy parameter, and this does not match the constant shape of the polarization spectrum during the burst. In addition, the density of the background plasma in the model and X–ray data are mismatches as it is three to five times higher than the estimates derived from the GOES and RHESSI data. A similar mismatch was reported by Fleishman *et al.* (2016) for a subclass of flares, but in these cases the radio and X–ray emissions were produced by distinct loops. Thus, we conclude that a polarization reversal through the beam–like anisotropy is unlikely in this event.

We consider the possibility that the ordinary wave in the optically thin mode is observed because it crosses a QT layer on the way from source 1 to Earth. An unipolar right–handed source at 17 GHz was observed at the place of source 1 from July 4 (Figure 5). A day before the flare, its sense of polarization reversed, and this can be regarded as a signature of a QT layer formation. In this case, the angle between the magnetic field vector and the line of sight must achieve 90 degrees somewhere along the propagation path, and the critical frequency f_t must exceed 35 GHz there. The critical frequency is determined by plasma parameters in the layer $f_t \simeq 7.6(N_{10}B_{100}^3 L_9)^{0.25}$ GHz, where N_{10} is the thermal density, expressed in the units of 10^{10} cm^{-3}; B_{100} is the magnetic field, expressed in units of 100 G; and L_9 is the scale of the angle changing, expressed in units
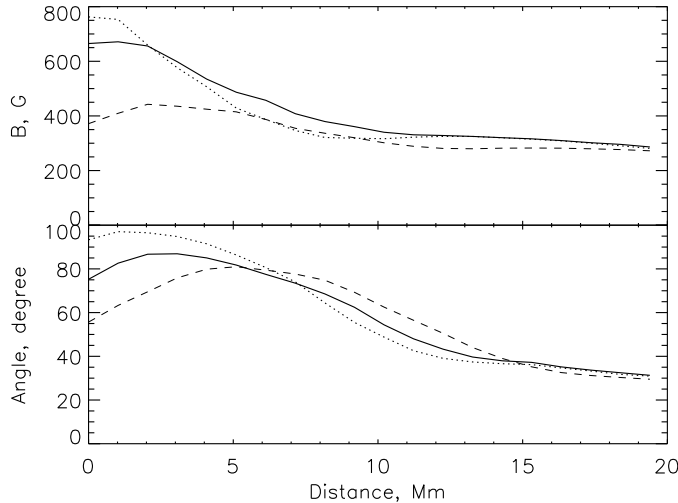
Figure 7. Height dependences of the magnetic field magnitude and the angle between its direction and the line of sight toward source 1 calculated for three points. The solid line corresponds to the line that starts from the 34 GHz brightness center, the dotted line shows the region three arcseconds to the east, and the dashed lines show the regions three arcseconds to the south.

of 10^9 cm (Zheleznyakov and Zlotnik, 1963). It has the strongest dependence on the magnetic field value.

We reconstructed the coronal magnetic field in the nonlinear force–free approximation, using an SDO/HMI vector magnetogram as input data. The field reconstruction was performed by the optimization method, proposed by Wheatland *et al.* (2000). In the study we used the implementation of the method developed by Rudenko and Myshyakov (2009). The magnetic field magnitudes calculated along the lines of sight are shown in Figure 7 (top panel). The different curves represent extrapolations for three points of source 1. The solid curve corresponds to the line of sight and starts from the 34 GHz brightness center, while the other curves begin at the points shifted three arcseconds toward east or south. The QT layer most likely exists at heights below 5 Mm where the magnetic field $B > 500$ G. This height is in accordance with the size of the small loop. The distance between the footpoints of the small loop was about 15 arcsec, so the altitude of source 1 might indeed be below the 5 Mm height. Magnetic field and plasma density in the QT layer may be sufficient to reverse the polarization height at frequencies of up to 35 GHz if the layer height is about 5 Mm.

In the case of the QT reversal we fit the microwave spectrum using an isotropic angular distribution of emitting electrons. One of the best fits is shown by the solid curve in Figure 2 (panel 3). Here we assumed that $f_t > 35$ GHz, and we show the calculated spectrum in polarization with the opposite sign. The observed spectrum can clearly be modeled with the reasonable fitting parameters: a source size is $3 \times 3 \times 5$ arcsec, plasma density 3×10^{10} cm^{-3}, power–law index

is $\delta_{MW} = 3.0$, density of the nonthermal electrons is 4.5×10^7 cm^{-3}, magnetic field is 610 G, and viewing angle is 80°.

4. Conclusions

Spatially resolved microwave polarization observations can provide important data on flare topology and plasma parameters. We have studied the flare SOL2012-07-06T01:37 which is a good illustration of a flare initiated by the interaction of a large and a small loop. The interaction site is seen as the main flare source in X–rays and microwaves and is characterized by an unusual behavior of the polarization spectrum: the wave type changes from extraordinary mode to ordinary mode at a frequency between 17 and 35 GHz. We have identified two possible reasons for the observed reversal of polarization sense. First, it could be due to a pitch–angle anisotropy of the emitting electrons. The scenario in which the electrons are strongly beamed places the source above 5 Mm and requires a dense loop there, which is not confirmed by either X–ray or EUV data.

On the other hand the spectrum fitting shows that the polarization reversal can be explained by the transition of gyrosynchrotron emission from the optically thick to thin mode. The observed circular polarizations are opposite to the intrinsic polarizations and can be reversed by the quasi–transverse effect. The quasi-transverse (QT) scenario places the source relatively low in the corona, which releases the stringent requirements on the thermal number density and nonthermal electrons, given that the magnetic field is reasonably large there. Recently, Sadykov *et al.*, 2016 reported a flare that occurred in a system of a low–lying loop arcade with a height of ≤ 4.5 Mm using *New Solar Telescope* (NST) data. Wang *et al.* (2017) reported a similar finding for flare precursors using a combination of NST and EOVSA data. We conclude that flares occurring in rather low–lying loops may not be unusual.

5. Acknowledgements

References

Alissandrakis, C.E., Nindos, A., Kundu, M.R.: 1993, *Solar Phys.* **147**, 343. ADS. DOI.
Altyntsev, A.T., Fleishman, G.D., Huang, G.-L., Melnikov, V.F.: 2008, *Astrophys. J.* **677**, 1367. ADS. DOI.

Altyntsev, A., Meshalkina, N., Mészárosová, H., Karlický, M., Palshin, V., Lesovoi, S.: 2016, *Solar Phys.* **291**, 445. ADS. DOI.

Aptekar, R.L., Frederiks, D.D, Golenetskii, S.V. Ilynskii, V.N., Mazets, E.P., Panov, V.N., Sokolova, Z.J., Terekhov, M.M., Sheshin, L.O., Cline, T.L., Stilwell, D.E.: 1995, *Space Sci. Rev.* **71**, 265. ADS. DOI.

Bastian, T.S., Benz, A.O., Gary, D.E.: 1998, *Annu. Rev. Astron. Astrophys.* **36**, 131. ADS. DOI.

Bastian, T.S.: 2004, *Solar and Space Weather Radiophysics, Astrophys. Space Sci. Lib.* **314**, 47. ADS. DOI.

Cohen, M.H.: 1960, *Astrophys. J.* **131**, 664. ADS. DOI.

Dulk, G.A.; Marsh, K.A.: 1982, *Astrophys. J.* **259**, 350. ADS. DOI.

Fleishman, G.D., Altyntsev, A.T., Meshalkina, N.S.: 2013, *Pub. Astron. Soc. Japan* **65**, S7. ADS. DOI.

Fleishman, G.D., Kuznetsov, A.A.: 2010, *Astrophys. J.* **721**, 1127. ADS. DOI.

Fleishman, G.D., Melnikov, V.F.: 2003, *Astrophys. J.* **587**, 823. ADS. DOI.

Fleishman, G.D., Nita, G.M., Kontar, E.P., Gary D.E.: 2016, *Astrophys. J.* **826**, 38F. ADS. DOI.

Fleishman, G.D., Palshin, V.D., Meshalkina, N.S., Lysenko, A.L., Kashapova, L.K., Altyntsev, A.T.: 2016, *Astrophys. J.* **822**, 71F. ADS. DOI.

Gary, D.E., Hurford, G.J.: 1994, *Astrophys. J.* **420**, 903. ADS. DOI.

Gary, D.E., Nita, G.M., Sane, N.: 2012, *AAS Meeting* **220**, Abstract id.204.30. ADS.

Grechnev, V.V.: 2003, *Solar Phys.* **213**, 103. ADS. DOI.

Grechnev, V.V., Lesovoi, S.V., Smolkov, G.Ya., Krissinel, B.B., Zandanov, V.G., Altyntsev, A.T., Kardapolova, N.N., Sergeev, R.Y., Uralov, A.M., Maksimov, V.P., Lubyshev, B.I.: 2003, *Solar Phys.*, **216**, 239. ADS. DOI.

Guidice, D.A., Cliver, E.W., Barron, W.R., Kahler, S.: *Bull. Am. Astron. Soc.* **13**, 553. ADS.

Hanaoka, Y.: 1997, *Solar Phys.* **173**, 319. ADS. DOI.

Huang, G., Nakajima, H.: 2009, *Astrophys. J.* **696**, 136. ADS. DOI.

Lee, J.,White, S.M., Kundu, M.R., Mikic, Z., McClymont, A.N.: 1998, *Solar Phys.* **180**, 193L. ADS. DOI.

Lemen, J.R., Title, A.M., Akin, D.J., Boerner, P.F., Chou, C., Drake, J.F. et al.: 2012, *Solar Phys.* **275**, 17. ADS. DOI.

Lesovoi, S.V., Altyntsev, A.T., Ivanov, E.F., Gubin, A.V.: 2014, *Research in Astronomy and Astrophysics* **14**, 864. ADS. DOI.

Lesovoi, S.V., Altyntsev, A.T., Kochanov, A.A., Grechnev V.V., Gubin A.V., Zhdanov D.A., Ivanov E.F., Uralov A.M., Kashapova L.K., Kuznetsov A.A., Meshalkina N.S., Sych R.A.: 2017, *Solar - Terrestrial Physics* **3**(1), 3. ADS. DOI.

Lin, R.P., Dennis, B.R., Hurford, G.J., Smith, D.M., Zehnder, A., Harvey, P.R. and 64 coauthors: 2002, *Solar Phys.* **210**, 3. ADS. DOI.

Lingenfelter, R.E., Ramaty, R.: 1967, *Planet. Spa. Sci.* **15**, 1303. ADS. DOI.

Morgachev, A.S., Kuznetsov, S.A., Melnikov, V.F.: 2014, *Geomagn. Aeron.* **54**, 933. ADS. DOI.

Nakajima, H., Nishio, M., Enome, S., Shibasaki, K., Takano, T., Hanaoka, Y., Torii, C., Sekiguchi, H., Bushimata, T., Kawashima, S., Shinohara, N., Irimajiri, Y., Koshiish, H., Kosugi, T., Shiomi, Y., Sawa, M., Kai, K.: 1994, *Proc. IEEE* **82**(5), 705. ADS.

Nishio, M., Yaji, K., Kosugi, T., Nakajima, H., Sakurai, T.: 1997, *Astrophys. J.* **489**, 976 ADS. DOI.

Palshin, V.D., Charikov, Yu.E., Aptekar, R.L., Golenetskii, S.V., Kokomov, A.A., Svinkin, D.S., Sokolova, Z.Ya., Ulanov, M.V., Frederiks, D.D., Tsvetkova, A.E.: 2014, *Geomagn. Aeron.* **54**, 943. ADS. DOI.

Ramaty, R.: 1969, *Astrophys. J.* **158**, 753. ADS. DOI.

Rudenko, G.V., Myshyakov, I.I.: 2009, *Solar Phys.* **257**, 287. ADS. DOI.

Ryabov, B.I., Maksimov, V.P., Lesovoi, S.V., Shibasaki, K., Nindos, A., Pevtsov, A.: 2005, *Solar Phys.* **226**, 223. ADS. DOI.

Sadykov, V.M., Kosovichev, A.G., Sharykin, I.N., Zimovets, I.V., Vargas Dominguez, S.: 2016, *Astrophys. J.* **828**, 4S. ADS. DOI.

Scherrer, P.H., Schou, J., Bush, R.I., Kosovichev, A.G., Bogart, R.S., Hoeksema, J.T., Liu, Y., Duvall, T.L., Zhao, J.; Title, A.M.: 2012, *Solar Phys.* **275**, 207. ADS. DOI.

Torii, C., Tsukiji, Y.,S.,K., Yoshimi, N., Tanaka, H., Enome, S.: 1979, *Proc. of the Res. Ist. of Atmospherics, Nagoya Univ.* **26**, 129 ADS.

Trottet, G., Krucker, S., Luthi, T., Magun, A.: 2008, *Astrophys. J.* **678**, 509. ADS. DOI.

Wang, H., Liu, C., Ahn, K., Xu, Y., Jing, J., Deng, N., Huang, N., Liu, R., Kusano, K., Fleishman, G.D., Gary, D.E., Cao, W.: 2017, *Nat. Astron.* **1**, 0085. ADS. DOI.

Wheatland, M.S., Sturrock, P.A., Roumeliotis, G.: 2000, *Astrophys. J.* **540**, 1150. ADS. DOI.

Yan, Y., Wang, W., Liu, F, Geng, L., Chen, Z., and Zhang, J: 2013, *Solar and Astrophysical Dynamos and Magnetic Activity, IAU Symposium* **294**, 489. ADS. DOI.

Zheleznyakov, V.V., Zlotnik, E.Ya.: 1963, *Astronomicheskii Zhurnal* **40**, 633. ADS.